The photoactive nitrogen impurity in nitrogen-doped zirconium titanate (N-ZrTiO4): A combined electron paramagnetic resonance and density functional theory study

Journal Name

ARTICLE

The Photoactive Nitrogen Impurity in Nitrogen-doped Zirconium Titanate (N-$ZrTiO_4$): A Combined Electron Paramagnetic Resonance and Density Functional Theory Study

Received 00th January 20xx,
Accepted 00th January 20xx

DOI: 10.1039/x0xx00000x

www.rsc.org/

Valeria Polliotto[a], Elisa Albanese[b], Stefano Livraghi[*a], Gianfranco Pacchioni[b] and Elio Giamello[a]

Nitrogen doping represents an important strategy to modulate the optical, magnetic and photochemical properties of the oxides for applications spanning from photocatalysis to optoelectronics and spintronics. In this work for the first time zirconium titanate, a material that exhibits many attractive properties including excellent dielectric constant, high corrosion resistance, high permittivity at microwave frequencies and excellent temperature stability, has been doped with nitrogen via a wet chemistry method. A detailed description of the geometrical and the electronic structure of the dopant centre has been obtained coupling Electron Paramagnetic Resonance (EPR) spectroscopy and density functional theory (DFT) calculations. Insertion of a nitrogen impurities in the $ZrTiO_4$ lattice modifies the optical properties causing an appreciable absorption in the visible range. The joint analysis of the EPR evidences and the DFT elaboration indicates that the nitrogen impurities preferentially occupy an interstitial position of the lattice generating, intra band gap states about 1 eV above the valence band edge that are responsible for the visible light absorption. The majority of intra band gap the states are diamagnetic (N^-) while a minor fraction is paramagnetic ($N^\bullet$). These centres are photosensitive in that the ratio between N^- and $N^\bullet$ is modified, upon irradiation, because of electron excitation from the intra band gap states to the conduction band.

1. Introduction

The incorporation of nitrogen impurities in oxides is becoming an important topic in several contexts of material chemistry research spanning from photocatalysis[1] to optoelectronics[2] and spintronics.[3] Insertion of nitrogen in the oxide lattice, in fact, represents a strategy to modulate the optical, magnetic and photochemical properties of the material.

As to the field of photocatalysis, a lot of efforts has been devoted, in the recent past, to dope, with this chemical element, titanium dioxide and several other oxides. In all these cases, aim of the doping was to extend the photoactivity of these materials, which usually are activated by the UV component of the light, to the visible wavelengths range. In most metal oxides the N impurities, introduced in the solid, usually form intra band gap states, just above the valence band, from which the electron excitation in the conduction band can be promoted also by visible light.[1,4,5] In spite of the huge number of papers concerning this important research field, some fundamental aspects such as the chemical nature of the dopant centres are still debated .

Incorporation of N atoms in an oxide lattice has also been proposed to be an effective way, with respect to the conventional cation substitution, to achieve p-type doping in oxide materials, which is fundamental for optoelectronic applications. In semiconducting oxides the N substitution for O in principle creates an electron deficient state with respect to the lattice O^{2-} introducing one hole per N situated just above the valence band chemical potential.[6]

Doping of nitrogen into tantalum pentoxide (Ta_2O_5) for instance, has been recently reported to have a dual-effect. The former is the visible light sensitization of this material for the photoelectrochemical hydrogen production by water splitting and the second is a change in the electronic structure that turns from n-type to p-type.[7]

The possibility of modifying the electronic structure of an oxide and, in particular, of obtaining p-type oxides moving from n-type materials, however still represents an highly questionable topic.[8,9] Some of us, for instance, have recently shown that in the case on SnO_2, for which the possibility to obtain a stable p-type SnO_2 would have a huge impact on the fabrication of various kinds of optoelectronic devices, the doped material is still rich in excess electrons as a result of its higher propensity to lose oxygen that is, in turn, determined by the presence of low lying N states in the band structure. This evidence suggests that the chance to prepare a p-type form of tin oxide, at least via nitrogen doping, is extremely low.[10]

[a] Dipartimento di Chimica and NIS, Università di Torino, Via P. Giuria 7, 10125 Torino, Italy.
[b] Dipartimento di Scienza dei Materiali, Università Milano Bicocca, via R. Cozzi 55, 20125 Milano, Italy.
stefano.livraghi@unito.it

Electronic Supplementary Information (ESI) available: [details of any supplementary information available should be included here]. See DOI: 10.1039/x0xx00000x

Intensive research efforts have been carried out by several researchers on exploring the effects of dilute doping of magnetic impurities on the physical properties of various oxides.[11] In these materials, nitrogen incorporation has been predicted to promote the onset of magnetic moments and ferromagnetic ordering at room temperature.[12] Once more, such an effect is related to the substitution of nitrogen for oxygen leading to holes in N 2*p* states, which form local magnetic moments. Both experimentally and theoretically, ferromagnetism has been recently proposed for different kinds of nitrogen doped oxides such as N-ZnO,[13] N-TiO_2,[14] N-In_2O_3,[15] N-$BaTiO_3$[16] and N-ZrO_2.[17] However, the nature and the origin of the ferromagnetism in doped semiconductors are often controversial.[18,19]

For all these reasons, several research groups are thus attempting to incorporate significant concentrations of nitrogen in oxide thin films, single crystals, and polycrystalline materials in order to achieve specific p-type doping, visible light active photocatalysts, or high temperature magnetic ordering. To optimize these efforts, however, it is important to understand the fundamental characteristics of nitrogen in these emerging technologically important materials.

Over the past decade some of us have used a combination of electron paramagnetic resonance (EPR) spectroscopy and density functional theory (DFT) calculations to characterize some of these fundamental aspects in several nitrogen containing polycrystalline oxides.[5,10,18,20-25]

EPR spectroscopy is, in fact, the technique of reference for the characterization of point defects in oxides and other non metallic materials since many of these defects are paramagnetic or can be excited to a paramagnetic state. EPR provides valuable information on the symmetry of the defect and often allows the evaluation of the electron spin density on the defect itself and on the surrounding atoms.[26,27] This information is of capital importance but not always sufficient to fully determine the structure of the defects centre in every detail. To achieve this final goal, a combination with advanced computational methods is essential since the direct comparison of the structural and electronic parameters of various possible models usually allows to understand which of them is compatible with the experimental findings.

In the present paper we turn our attention to zirconium titanate ($ZrTiO_4$), a material that exhibits many attractive properties including excellent dielectric constant, high corrosion resistance, high permittivity at microwave frequencies and excellent temperature stability.[28-31] For these reasons this oxide is widely used in technological applications. In this work, for the first time, nitrogen was introduced in the $ZrTiO_4$ crystal structure using wet-chemistry methods. The consequences on the electronic and magnetic properties of the solid have been studied with EPR and DFT.

2. Experimental methods

Sample preparation: Al reactants were purchased by Sigma-Aldrich and were employed without any further treatment. N-$ZrTiO_4$ powders (hereafter N-ZT) were prepared mixing a solution of 1.75 mL of titanium(IV) isopropoxide (97%) in 1.75 mL of 2-propanol alcohol (>99.8%) and a second water solution prepared with 2 g of $ZrOCl_2$•$8H_2O$ (99.9%), 0.14 g of NH_4Cl (99.998%) and 5 mL of water. The resulting mix was stirred at room temperature until a transparent solution was obtained. The solution was left to age for 15 hours at room temperature and subsequently dried at 343 K. Finally the dried material was calcined in air at 773 K for 1 hour. The powders so obtained have a yellow colour and a specific surface area, for various batch, around 12 m^2/g A material enriched with the ^{15}N isotope (^{15}N-$ZrTiO_4$) was prepared in the same way previously described using 98% ^{15}N enriched NH_4Cl.

X-Ray Diffraction: Powder X-ray diffraction (XRD) pattern was recorded by a PANalytical PW3040/60 X'Pert PRO MPD diffractometer using a copper Kα radiation source (0.154056 nm). Diffraction patterns were refined with Rietveld method using MAUD (Material Analysis Using Diffraction) program.[32,33]

UV-vis absorbance: The UV-vis absorption spectra were recorded using a Varian Cary 5 spectrometer, coupled with an integration sphere for diffuse reflectance studies, using a Carywin-UV/scan software. A sample of PTFE with 100% reflectance was used as the reference.

Surface area measurements: The surface area measurement was carried out on a Micromeritics ASAP 2020 apparatus using the Brunauer–Emmett–Teller (BET) model for N_2 adsorption measurements. Prior to the adsorption run, the sample was outgassed at 573 K for 2 h.

UV-vis irradiation: The samples were irradiated using a 1600 W xenon lamp (Oriel instruments) equipped with a IR water filter and:
a) a cut-off filter λ > 420 nm for polychromatic irradiation,
b) a grating monocromathor with a transmission range between 500 and 180 nm for monochromatic irradiation.
Irradiance was measured in all experiments by a Deltahom instrument equipped with a detector for the vis−NIR range (400−1050 nm, measuring range 0.1−2000 W/m^2). The effect of irradiation on EPR spectra was investigated irradiating the sample in the EPR cavity at RT.

EPR characterization: Continuous Wave Electron Paramagnetic Resonance (CW-EPR) experiments were performed using a Bruker EMX spectrometer operating at X-band (9.5 GHz), equipped with a cylindrical cavity operating at 100 kHz field modulation. All the spectra were recorded with a Modulation Amplitude 0.2 mT, microwave power of 1 mW and at room temperature.
Q-band continuous wave (CW) EPR spectra have been recorded at room temperature (RT) on a Bruker ELEXYS 580 operating at a 50 kHz field modulation. A spin counting was performed comparing the intensities of the N-$ZrTiO_4$ samples with those of freshly prepared DPPH solutions in cyclohexane. The computer program SIM32[34] was used for spectral simulation.

Computational Methods: The investigation of N-$ZrTiO_4$ was carried out with periodic density functional theory (DFT) calculations employing the hybrid B3LYP [35,36] functional as implemented in CRYSTAL14 code.[37] Crystalline orbitals were represented as linear combinations of Bloch functions (BF) and were evaluated over a regular three-dimensions mesh of points in reciprocal space. Each BF was built from local atomic orbitals (AO) resulting from contractions of Gaussian-type functions, which in turn are the product of a Gaussian times a real solid spherical harmonic function. All electron basis sets for O (8-411(d1)), N (7-311(d1)) and Ti (86-411(d41)) have been used. For Zr, a 311(d1) basis set associated to ECP (Hay and Wadt small-core potential)[38] has been adopted. For the numerical integration of exchange-correlation term, 75 radial points and 974 angular points (XLGRID) in a Lebedev scheme in the region of chemical interest were adopted. The Pack-Monkhorst/Gilat shrinking factors for the reciprocal space were set to 3 for all the structures, which correspond to 14 real reciprocal space points at which the Hamiltonian matrix was diagonalized.
A 2x2x1 supercell of orthorhombic $ZrTiO_4$ containing 48 atoms has been modeled. This allows having a N dopant percentage of 3.1%. The accuracy of the integral calculations was increased with respect to its default value by setting the tolerances to 7, 7, 7, 7 and 18. The self-consistent field (SCF) iterative procedure converged to a tolerance in total energy of $\Delta E = 1 \cdot 10^{-6}$ a.u.. The above computational parameters ensured a full numerical convergence on all the computed properties. All the crystal structures are fully optimized (i.e. both cell parameters and internal coordinates) without symmetry operators.

3. Results and discussion

3.1 Structural and optical characterizations

The XRD diffractogram, with the corresponding computer simulation, and the UV-vis diffuse reflectance spectrum of a N-ZT sample are reported in Figure 1. The Rietveld refinement of the XRD pattern (Fig. 1A) shows beside, a small fraction of anatase (c.a. 2%) and tetragonal ZrO_2 (c.a. 1.3%), the formation of crystals of $ZrTiO_4$ with the typical scrutinyite structure. In this structure, somehow similar to those of the main TiO_2 polymorph (rutile, anatase, brookite), the MeO_6 octahedra are connected by tricoordinated oxygen atoms. However, the symmetry of the structure (space group *Pbcn*) is different from those of the polymorphs of titanium dioxide and the MeO_6 octahedra contain, with a random distribution, either titanium or zirconium.[39]
Figure 1B reports the UV-vis absorption spectrum of N doped $ZrTiO_4$ (N-ZT) sample. The characteristic absorption edge in the UV region, due to the electron transfer from the valence band to the conduction band is observed. The optical band gap absorption obtained by means of a Tauc plot indicates that the optical band gap of the N-ZT sample is unchanged with respect to the undoped material. Assuming a direct transition, as in the case of bare $ZrTiO_4$ [40], the band gap energy (E_g) measured by the Tauc's plot method is, in fact, 3.6 eV. The optical properties of the N-ZT material however differ from those of the bare zirconium titanate for the broad absorption shoulder in the visible region centred at about 430 nm. The optical features reported in Figure 1B closely recall what occurs in the case of the nitrogen doped TiO_2 materials in which the doping procedure introduces intra band gap states that cause light absorption in the visible wavelength range.[24]

3.2 EPR characterization

Nitrogen doped zirconium titanate contains paramagnetic centres which are due to the nitrogen insertion in the diamagnetic matrix. This is clearly shown by the EPR spectra of the material, which were run at two distinct frequencies, 9.5 GHz (X-band) and 35 GHz (Q-band) (Fig. 2). The as prepared material shows a relatively low intensity EPR signal, for this reason all the spectra reported in Figure 2 were recorded after visible light irradiation in order to increase the signal to noise ratio (see section 3.4) and to obtain a more reliable analysis. The role of nitrogen in this paramagnetic defect is, first of all, argued from the typical three-lines hyperfine structure of the spectra containing N in natural abundance (essentially ^{14}N with nuclear spin I=1 and line multiplicity n = 2I+1= 3) and is also confirmed by isotopic substitution with ^{15}N. In this the case the signals change from three to two hyperfine lines according to the different nuclear spin of ^{15}N (I=1/2, n = 2).

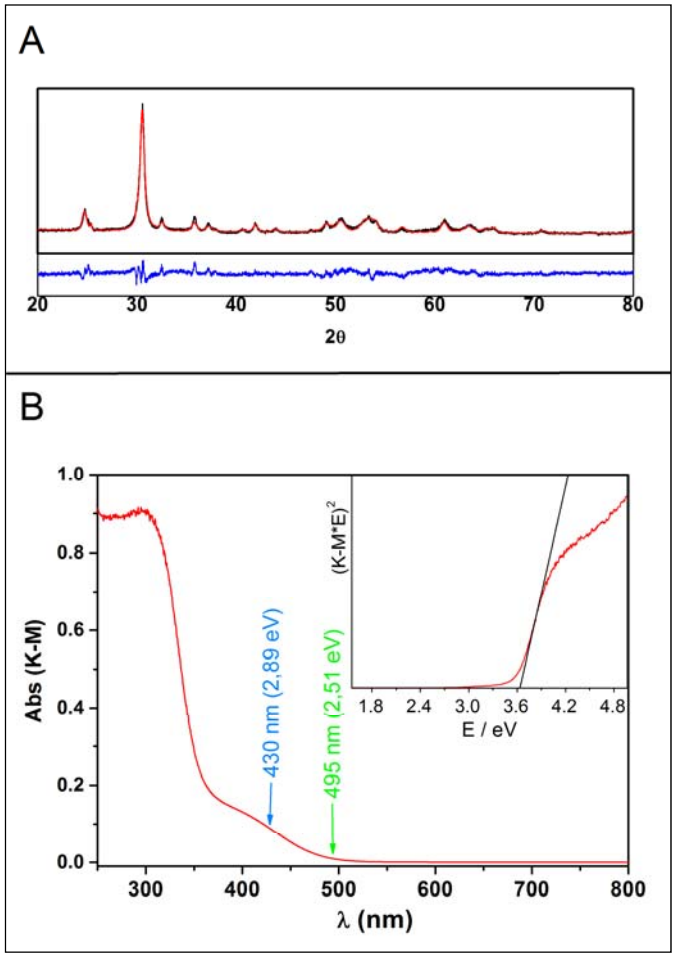

Figure 1. A) XRD pattern of N-ZT sample. Black line: experimental trace. Red line: computer simulation obtained by Rietveld refinement. Blue line: difference between experimental simulated patterns. B) UV-vis absorption spectrum of N-ZT sample. In the inset the Tauc's plot is reported.

The whole set of spectra reported in Figure 2 was simulated (red lines) on the basis of rhombic g and hyperfine A tensors having three *g* values very close one to each other in the range 2.0081-2.0038. The use of an higher frequency (Q-band) has the aim of increasing the separation between the various *g* features while those due to the electron nucleus interaction (hyperfine structure) are kept constant. The same set of spin-Hamiltonian parameters was used in the four simulations reported in Figure 2 just scaling the hyperfine coupling constant of the expected value passing from ^{14}N and ^{15}N which corresponds to the ratio of the two nuclear g_N factors of the two nuclei. The goodness of the fit between experimental and simulated spectra in the four distinct cases firmly indicates the quality of the obtained spin Hamiltonian parameters. The values of g and A tensor elements obtained by the described simulation are reported in Table 2. The signal is characterized by a hyperfine coupling tensor mainly concentrated in one direction.

The spin density on the nitrogen atom of the N centre can be derived from the hyperfine matrix A (Table 2) according to:

$$A = \begin{vmatrix} A_1 & 0 & 0 \\ 0 & A_2 & 0 \\ 0 & 0 & A_3 \end{vmatrix} = a_{iso} + \begin{vmatrix} 2T & 0 & 0 \\ 0 & -T & 0 \\ 0 & 0 & -T \end{vmatrix} = 1.260 + \begin{vmatrix} 2.138 & 0 & 0 \\ 0 & -1.040 & 0 \\ 0 & 0 & -1.097 \end{vmatrix} \quad (1)$$

where a_{iso} is the Fermi contact term (proportional to the 2s electron spin density in the nuclear volume) and T is the dipolar matrix having the typical form of the electron-nucleus dipolar interaction for an electron in a p orbital (i.e., *2T*, *-T*, *-T*). The spin density in the *p* orbital, ρ_{2p}, calculated by comparison of the experimental dipolar value with the corresponding atomic one (ρ_{2p}= *T*/*T*°) is ρ_{2p} =0.67 (*T*° = 1.816 mT [41]). The isotropic Fermi contact term is expected to be positive in N-centred radical species and indicates a further amount of electron spin density (0.020) in the 2*s* orbital of the nitrogen atom. The total spin density on the N atom of the observed species amounts therefore to 0.69, with the larger contribution being due to a single 2*p* orbital.

Comparing the set of data obtained for the N-ZT sample with data reported for other paramagnetic species involving nitrogen in different oxide matrices, the following considerations can be done: i) The spin-Hamiltonian parameters reported in Table 2 let to exclude, in N-ZT, the assignment of the EPR spectra either to trapped molecular species (such as nitrogen oxides, NO and NO_2), as occurs in other nitrogen doped oxides[42] or to the presence of diatomic N-species as reported for example in the case of N-MgO or N-ZnO.[22,43] ii) In the N-ZT materials a tiny amount of TiO_2 is segregated during the preparation procedure. However, on the basis of both the spectral intensity and the hyperfine constant value (the spectral shape is similar in the two cases, but the main hyperfine values are definitely higher in the case of $ZrTiO_4$), the contribution of N centres in TiO_2 to the observed EPR spectra can be confidently excluded. iii) The previous analysis also shows that the nitrogen hyperfine tensor does not account for the whole unpaired electron spin density. In other words, a fraction of the spin density is likely localized on other nuclei having zero nuclear spin. This evidence suggest that the nitrogen containing species strongly interacts with the oxidic matrix as expected for an atom that replaces the lattice oxygen (substitutional nitrogen) or for an atom in interstitial arrangement as it was found in the case of N-TiO_2.[20] For sake of simplicity, hereafter the paramagnetic nitrogen species in zirconium titanate will be denoted as $N^{\bullet}$.

g tensor	^{14}N **A** tensor (mT)	^{15}**N A** tensor (mT)
g_z = 2.0081 ± 0.0001	A_z = 0.22 ± 0.09	A_z = 0.32 ± 0.09
g_y = 2.0046 ± 0.0003	A_y = 3.40 ± 0.06	A_y = 4.90 ± 0.06
g_x = 2.0038 ± 0.0002	A_x = 0.16 ± 0.01	A_x = 0.26 ± 0.01

Table 1. g and hyperfine A tensors of the nitrogen center in $ZrTiO_4$ extracted by simulation of the experimental spectra.

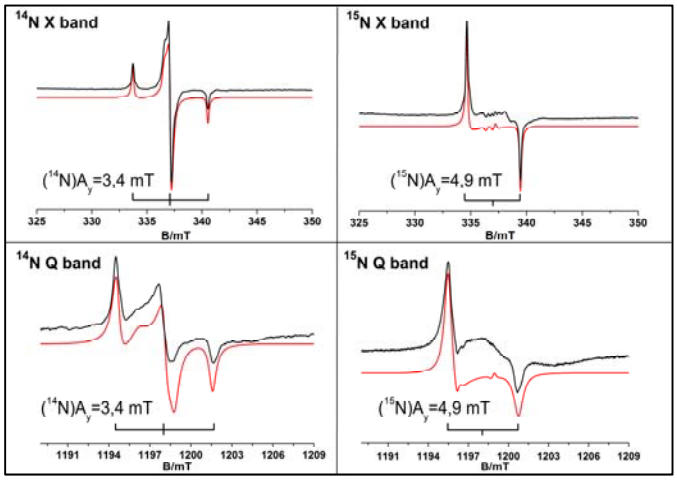

Figure 2. X and Q band experimental (black) and simulated (red) EPR spectra of ^{14}N-ZT and ^{15}N-ZT samples recorded at RT. All the spectra were recorded after irradiation with visible light (λ > 420 nm) in order to get a better signal to noise ratio, as will be shown in the following section (§3.4).

3.3 DFT Calculations

As reported on our previous work on the electronic and structure properties of $ZrTiO_4$,[40] Ti and Zr ions, which can randomly occupy half of the cation octahedral sites of the scrutinyite structure, assume preferentially a dispersed configuration over a segregated one. Therefore, a dispersed configuration has been adopted for the present calculations (see ESI, Fig. S1). The computed cell parameters are in good agreement with the experimental ones and the Kohn-Shan band gap results overestimated because of the Ti component. In fact, the B3LYP functional tends to overestimate the TiO_2 band gap by about 21%. By applying this correction, we obtain E_g = 3.8 eV, rather close to the experimental value (see Ref. 40 for details).

The $N^{\bullet}$ dopant has been inserted as substitutional to O, N_{sub}, and as interstitial, N_{int}. Several O species characterized by different coordination spheres are present in the $ZrTiO_4$ structure (see ESI, Fig. S1); consequently, several N_{sub} and N_{int} configurations can, in principle, be modelled. In particular, we

simulated two substitutional (N_{sub}-$ZrTiO_4$) and two interstitial (N_{int}-$ZrTiO_4$) models.

As regards N_{sub}-$ZrTiO_4$, N is substitutional to an O_{4c} (4-coordinated O) atom bound to one Ti and three Zr atoms (i.e. N_{sub4c}-$ZrTiO_4$) and to an O_{3c} surrounded by two Ti and one Zr (N_{sub3c}-$ZrTiO_4$). In the former, during the optimization process of the bare structure (see Ref. 40 for details), in the case of O_{3c} oxygen directly bound to three Zr cations, a slight modification of the coordination sphere occurs with formation of a tetracoordinated oxygen ion. When this kind of oxygen is

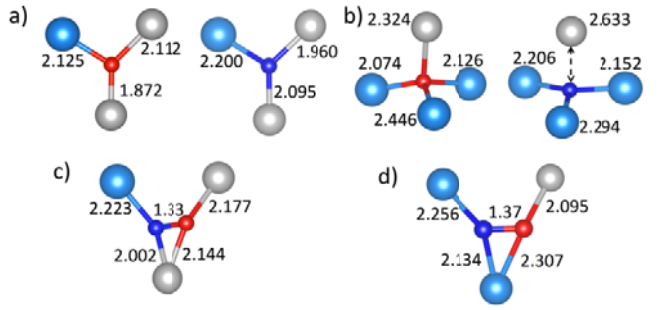

Figure 3. Local structural features of a) pure $ZrTiO_4$ (left) and N_{sub3c}-$ZrTiO_4$ (right), b) pure $ZrTiO_4$ (left) and N_{sub4c}-$ZrTiO_4$ (right), c) N_{int1}-$ZrTiO_4$ and d) N_{int2}-$ZrTiO_4$ (d). Bond lengths are in Å. Zr atoms are represented in light blue, Ti in gray, O in red and N in blue.

replaced by nitrogen the resulting N_{sub4c} modifies its coordination sphere moving away from the Ti atom, thus becoming again planar tricoordinated (Fig. 3b). On the contrary, the N_{sub3c} substitution does not affect the geometry (Fig. 3a). The two substitutional structures have very similar stability.

The interstitial N dopants have been inserted in the middle of two different cavities and, in both cases at the end of the relaxation process they form a N-O species with an O_{3c} atom (N_{int1}-$ZrTiO_4$ and N_{int2}-$ZrTiO_4$, Fig. 3).

In Figure 4 the total and projected density of states for N and the neighboring Zr, Ti and O atoms (see labels in Figure 4, TiN, ZrN and ON) of all the defective structures are reported. The N_{sub} dopant does not strongly affect the local geometry and introduces a singly occupied N $2p_\alpha$ state, which lies just above the O 2p states. The corresponding empty $2p_\beta$ component (hole state) is fully localized and lies about 1.2 eV below the bottom of the conducting band (CB) (see Fig. 4).

The interstitial dopant is associated with a NO π molecular orbital, as observed for other doped oxides, such as N_{int}-TiO_2, N_{int}-ZrO_2 and N_{int}-SnO_2.[18,24,25] Here, the spin density (ρ) is localized on the π system, thus reducing the localization on $N^\bullet$ from 0.9 (ρ in N_{sub}) to about 0.8 (see Table 2). The presence of $NO^\bullet$ species introduce singly occupied NO $\pi^*\alpha$ states, which lie above the top of the O 2p valence band (VB) by 1 eV and that are responsible of the EPR signals (Fig. 2). The hole state is localized on the empty $NO^\bullet$ π^*_β 0.5 eV below the CB.

The local structure surrounding the N_{int} atom does not influence its electronic behavior. On the contrary, it slightly affects the structure stability, being the N_{int1} more stable than the N_{int2} by about 0.2 eV.

Table 2 shows the hyperfine coupling constants (hfcc) for the four N-doped structures. For a direct comparison, also the

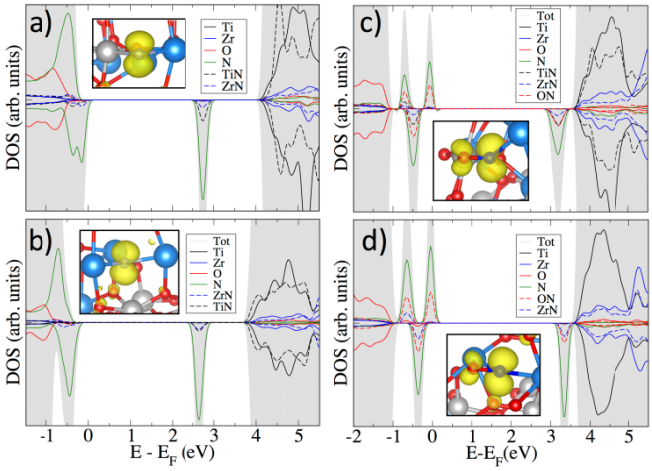

Figure 4. Total density of states (grey) and projected density of states of a) N_{sub3c}-$ZrTiO_4$, b) N_{sub4c}-$ZrTiO_4$, c) N_{int1}-$ZrTiO_4$ and d) N_{int2}-$ZrTiO_4$. The Fermi energy is set to the highest occupied level. In the inset the spin density plots are reported (isolevel cutoff 0.007 e/a.u.^{3}).

values of N-doped TiO_2 and N-ZrO_2 from previous studies are reported. The data obtained for the two substitutional structures (as well as for the two interstitials) are very similar, therefore, the hfcc of $N^\bullet$ dopant seems to be independent by the first coordination sphere. They are closer to N-ZrO_2 values than to N-TiO_2 ones, as observed experimentally (see Table 2).

However, the comparison between the substitutional and the interstitial hfcc show some relevant difference. In N_{sub}-$ZrTiO_4$, the anisotropic T tensor has the typical form of the electron-nucleus dipolar interaction for an electron in a *p* orbital (i.e $2T_1$, $-T_2$, $-T_3$) and a_{iso} has a value around 0.5 mT. On the contrary, in the interstitial cases, a slight asymmetry in the T tensor (T_2 and T_3 are quite different) is observed and a_{iso}, 0.9 mT, is almost twice as large compared to the N_{sub} ones, in good agreement with the experimental data.

In conclusion, N_{sub}-$ZrTiO_4$ and N_{int}-$ZrTiO_4$ hfcc exhibit small but significant differences in the T matrix and a_{iso} values, with the interstitial ones closer to the experimental values. This allow a tentative assignment of the N doped-$ZrTiO_4$ species to interstitial $N^\bullet$ dopants, that forms a N-$O^\bullet$ species with an O lattice atoms.

3.4 Photosensitivity of the $N^\bullet$ center in $ZrTiO_4$

In previous works carried out in our research group on nitrogen doped oxides, the study of these materials under irradiation has turned out to be essential to shed light on the effective role of the N containing species in the electronic structure of the doped oxides.[23, 24] For this reason, also in the present work, an EPR characterization of N-doped $ZrTiO_4$ sample under different condition of illumination has been carried out.

Bare $ZrTiO_4$ with an intrinsic band gap of 3.6 eV adsorbs UV wavelengths, as occur in mostly of the white transition metal oxides,[40] to promote valence band electrons in the conduction

	A_1	A_2	A_3	a_{iso}	T_1	T_2	T_3	ρ	ΔE
N_{sub4c}-$ZrTiO_4$	2.967	-0.686	-0.669	0.538	2.430	-1.224	-1.206	0.90	+0.05
N_{sub3c}-$ZrTiO_4$	2.994	-0.684	-0.660	0.550	2.444	-1.234	-1.210	0.90	0.0
N_{int1}-$ZrTiO_4$	**3.369**	**-0.358**	**-0.195**	**0.939**	**2.430**	**-1.296**	**-1.134**	**0.75**	**0.0**
N_{int2}-$ZrTiO_4$	**3.459**	**-0.510**	**-0.377**	**0.857**	**2.602**	**-1.367**	**-1.235**	**0.80**	**+0.17**
Expt	**±3.40**	**±0.22**	**±0.16**	**1.26**	**2.14**	**1.04**	**1.10**	**0.69**	
$N_{int}ZrO_2$	3.563	-0.612	-0.472	0.826	2.737	-1.438	-1.299	0.84	
$N_{int}TiO_2$	3.34	0.20	0.18	1.18	2.16	-1.16	-1.00	0.67	

Table 2: Computed and experimental ^{14}N hyperfine coupling constants (mT), spin densities and relative stabilities (eV) for all the defective structures. The values of N_{int}-TiO_2 and N_{int}-ZrO_2 are also reported.

band. The optical properties described in section 3.2 however indicate that the N-ZT material also shows some visible light absorption, which seems strictly related to the nitrogen doping.For this reason, it is important to monitor the effect of visible light irradiation, in particular on the EPR signal corresponding to the $N^{\bullet}$ centre. Figure 5 reports the intensity of the EPR signals of the $N^{\bullet}$ species upon polychromatic visible light irradiation (λ>420 nm).

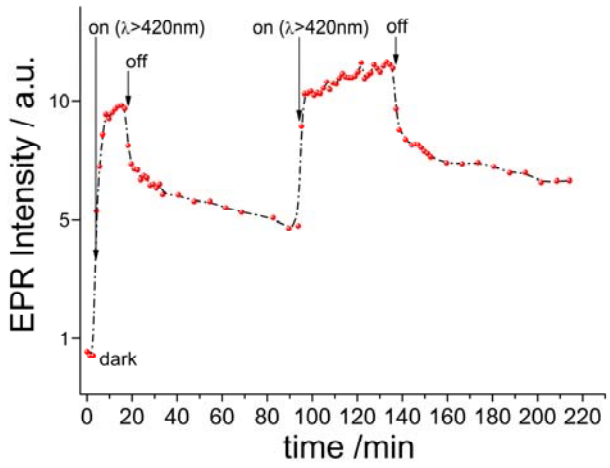

Figure 5. EPR signal intensity of $N^{\bullet}$ species under visible light irradiation (λ>420 nm).

Irradiating in this way the sample, kept under vacuum, the EPR signal of $N^{\bullet}$ rapidly grows of about one order of magnitude. When the irradiation source is turned off the signal intensity decreases (following an apparent exponentially decay) without recovering, in a time interval of one hour, the initial intensity. The described behaviour is reversible, and the signal grows when the light is turned on again (Fig. 5).

Considering the numerous similarities on the N-ZT sample with other doped oxides, the observed behaviour has to be ascribed to the interaction of visible light photons with the electrons of N defective states. More in detail the visible light (E ≤ 2.95 eV), which is actually ineffective on bare $ZrTiO_4$ and has not sufficient energy to promote electrons from the valence band to the conduction band (3.6 eV), excites electrons from the intra band gap state associated to the nitrogen impurity to the conduction band (CB). However, since the effect of the visible light absorption is a net increase of the EPR intensity of the paramagnetic $N^{\bullet}$ species, the operating mechanism at the origin of such phenomenon has to involve a diamagnetic counterpart (N^-) of the $N^{\bullet}$ centre (eq. 2). In other words the observed effect of the irradiation discloses the presence, beside the $N^{\bullet}$ centre of a diamagnetic counterpart, N^-.

$$N^-(\uparrow\downarrow) + h\nu(vis.) \rightarrow N^{\bullet}(\uparrow) + e^-(CB) \quad (2)$$

When the irradiation source is turned off the recombination (eq. 3) occurs:

$$N^{\bullet}(\uparrow) + e^-(CB) \rightarrow N^-(\uparrow\downarrow) \quad (3)$$

The increase of $N^{\bullet}$ intensity upon irradiation can be explained only assuming that N^- centres are more abundant than $N^{\bullet}$ ones and are therefore preferentially depopulated by selective irradiation as described by the equation 2. In Figure 5 it is also worth to note that, after turning off the irradiation source, the intensity of $N^{\bullet}$ centres, after a nearly exponential decay, does not recover the initial value but remains higher than the starting one after at least an hour. Considering that no other paramagnetic centres are observed during the excitation and relaxation steps, this implies that a fraction of the photoexcited electrons remains trapped, after irradiation in some diamagnetic form and so EPR silent. Something similar occurs in bare $ZrTiO_4$ for which the presence of EPR silent trapped electrons have been proved.[40] The EPR silent nature of these centres however makes the disclosing of their exact nature particularly puzzling. As predicted by the theoretical elaboration in other oxide as bare $ZrTiO_4$ and ZrO_2, most probably, this centers correspond to neutral vacancies (V_O^X) with two electrons simultaneously trapped in the defects.[18,40]

In order to better understand what component of the visible light spectrum is involved in $N^{\bullet}$ photoexcitation, irradiation experiments with monochromatic light have been also performed. Figure 6A reports the EPR spectra of N-ZT sample recorded under irradiation with two different monochromatic wavelengths, in the green (495 nm) and in the blue (430 nm) region of the visible spectrum respectively (Fig. 6A,a and 6A,b). The irradiation was performed applying a monochromator to the lamp obtaining an irradiance of 0.6 W/m^2 in the two cases. The first wavelength corresponds to the tail of the absorption band in the visible, while the second one corresponds to the maximum of this absorption (Fig. 1B). The effect of the two monochromatic wavelengths is also compared with that caused by the irradiation with polychromatic visible light (λ>420 nm) (Fig. 6A,c).

The irradiation of the sample with the green light causes a tiny increase of the $N^{\bullet}$ EPR signal intensity (Fig. 6A,a) with respect to the dark. A further growth of the signal takes place upon irradiation of

the sample with the blue light (Fig. 6A,b). However, the largest effect is observed when the sample is irradiated with polychromatic visible light (Fig. 6A,c). In Figure 6B the spin count (number of spin per gram of material) in different irradiation conditions is also reported. Inspection of Figure 6 indicates that: i) the EPR intensity of $N^{\bullet}$ species is poorly affected by illumination with green light in comparison to what happens with blue light. This behaviour is in agreement with the optical spectrum reported in Figure 1B where the maximum absorption occurs in the blue region. ii) using polychromatic light for the same amount of time, the growth in intensity of the $N^{\bullet}$ signal is much more pronounced. This latter fact is due to various reasons. First of all the irradiance of the whole lamp (λ>420 nm) is much higher than that obtained using the monochromator. Second, the effect of the polychromatic light (that includes NIR frequencies) results in a complex mechanism of excitation of the electrons involving transitions from valence band to intra band gap states, as already observed in similar cases.[24]

A disentanglement of all the contributions to the observed behaviour of the EPR intensity of $N^{\bullet}$ is beyond the purpose of the present paper. However, it remains true that, as shown by the experiment in Figure 6, the $N^{\bullet}$ species in $ZrTiO_4$ are visible light sensitive. Electrons from intra band gap states can be excited by visible frequency to the conduction band from which they slowly decay to the starting state when the irradiation is turned off.

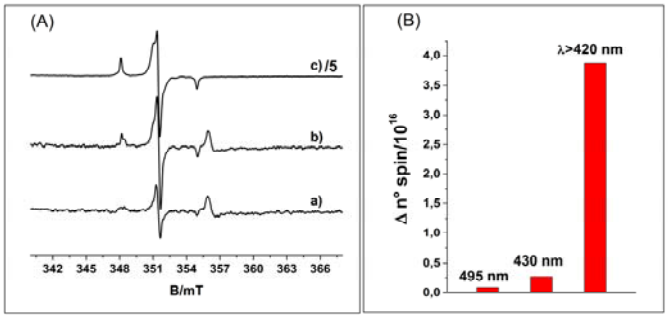

Figure 6. (A) EPR spectra of the N-ZT sample upon different irradiation condition: a) irradiated with green light (λ = 495 nm), b) irradiated with blue light (λ = 430 nm) and c) irradiated with polychromatic visible light (λ > 420 nm). (B) Differences of spins per gram of the $N^{\bullet}$ species after 10 minutes of irradiation with different light sources. The irradiance are 0.6 W/m^2 and >2000 W/m^2 for monochromatic light (blue and green) and polychromatic light (λ > 420 nm) respectively

The simultaneous presence and the interplay between diamagnetic (N^{-}) and paramagnetic ($N^{\bullet}$) intra band gap states is confirmed by thermal annealing under vacuum (773K) and reoxidation experiment at the same temperature. Upon thermal annealing in vacuum zirconium titanate (like other semiconducting oxides), looses oxygen resulting in excess electrons in the solid.[40] These are, at least in part, stabilized in the low-lying $N^{\bullet}$ centres.

The two following equations describe the phenomenon, which has been monitored in terms of a dramatic decrease of the EPR intensity of the $N^{\bullet}$ EPR signal (see ESI, Fig. S2).

$$ZrTiO_4 \rightarrow ZrTiO_{4-x} + \frac{x}{2} O_2 + xV_O^{\bullet\bullet} + 2e^- \quad (4)$$

$$2N^{\bullet}(\uparrow) + 2e^- \rightarrow 2N^{-}(\uparrow\downarrow) \quad (5)$$

Reoxidation in oxygen at the same temperature inverts the phenomenon (eq. 6) even thought, due to the low surface area of the material, the recovery of the starting EPR intensity is quite low. The experiment not only confirms the coexistence of two forms of the N impurity, but firmly indicates that these are crucial features of the electronic structure of the solid fully involved in the redox chemistry.

$$\frac{x}{2} O_2 + xV_O^{\bullet\bullet} + 2xN^{-}(\uparrow\downarrow) \rightarrow O^{2-} + N^{\bullet}(\uparrow) \quad (6)$$

The presence of both $N^{\bullet}$ and N^{-} species is in agreement with what observed for other N-doped oxides, such as N-TiO_2 and forecast on the basis of computational work in the case of N-ZrO_2 and N-BaO.[18, 19, 44] According to what reported for other N-doped oxides the simultaneously presence of the two forms of nitrogen ($N^{\bullet}$ and N^{-}) also indicate that the presence of the N dopants leads to a strong decrease of the cost of oxygen vacancy (V_O) formation (E_{form}). In the case of N-ZrO_2, E_{form} (computed with respect to ½ O_2) goes from 7.2 eV to less than 2 eV;[18] here the value decreases from 5.5 eV to 1.0 eV. This is related to the presence of acceptor species (the N impurity atoms with deep, singly occupied 2p states) that facilitates the formation of the oxygen vacancy. As a consequence, the two electrons associated to the V_O are transferred to two N 2p states and their magnetic moment is completely quenched resulting in a diamagnetic center. The corresponding energy levels lie at about 0.45 eV above the top of VB. Summarizing, the previous experiments together with the computational results point to the presence of intra band gap N-states some tenths of eV above the valence band edge. The majority of these states are diamagnetic (N^{-}) while a minor fraction is paramagnetic ($N^{\bullet}$) and allows a detailed EPR characterization.

3.5 The $N^{\bullet}$ center in $ZrTiO_4$ and other nitrogen doped oxides

The problem of N impurities in oxides is not easy to rationalize. First of all not all oxides are prone to incorporate nitrogen, at least via chemical synthesis. At first sight, on the basis of the examples available in the literature, it seems that the nitrogen incorporation, via chemical methods, is easier in materials containing low coordinated oxygen ions. The more popular examples of N doping are in fact found for the oxides having 3- or 4- coordinated oxygen ion as ZnO [23,43] (wurtzite structure, O_{4c}), TiO_2 rutile and anatase (O_{3c}),[1,24,45] WO_3[46-48] (monoclinic O_{2c}) and SnO_2 (rutile O_{3c}).[25,49,50]

In this work we have synthesized and investigated, for the first time, the N-doped $ZrTiO_4$ material with a simple and cheap wet chemistry method. The resulting solid shows a vivid yellow colour and the presence of a paramagnetic defect, which is due to a nitrogen-containing species. Different models of insertion of nitrogen in the $ZrTiO_4$ structure have been investigated by means of quantum mechanical calculations in order to achieve a full understanding of the electronic structure of the doped solid and a detailed microscopic structure model for the nitrogen defect. Coupling DFT and EPR investigation, it has been possible to assign the observed paramagnetic nitrogen impurity to a defect involving an interstitial form of nitrogen. In such defect, the nitrogen impurity is bound to a O atom leading to a N-O species with an unpaired electron occupying a NO π-type localized orbital.

In principle other situations are possible. Besides interstitial, also substitutional centres can be formed depending, *inter alia*, by the experimental conditions of the preparation. Calculated stability phase diagrams show that the ratio between the two types of impurities markedly vary as a function of the temperature and the oxygen partial pressure.[20] In the case here described (N-$ZrTiO_4$), the nitrogen centre clearly resembles that described in the case of TiO_2 (both anatase and rutile),[24,45] provided that the preparation method is similar. At first sight wet chemistry methods (precipitation, Sol-Gel etc...) seem to favour the formation of a N-O chemical bond.[51,52] At variance, always in the case of TiO_2, it is known that different methods (nitridation at high temperature, magneto sputtering etc…)[53-55] lead to the formation of substitutional N species as shown by XPS measurements. Notice that an EPR spectrum for this type of defects in TiO_2, has never been reported. The analogues behaviour of TiO_2 and $ZrTiO_4$ could be rationalized in terms of structural analogy of the two systems. $ZrTiO_4$ has an orthorhombic structure (*Pbcn*) where the titanium and zirconium ions are randomly distributed on equivalent octahedral sites and are surrounded by six oxygen atoms (MO_6) and the oxygen atoms are connected to three metals ions. These structural features are very similar to those of all TiO_2 polymorphs that are based on TiO_6 octahedra and a three coordinated (O_{3c}) lattice oxygen.

Further consideration can be drown comparing the results reported here with those described for other nitrogen doped oxides and in particular for the "parent" binary oxides, TiO_2 and ZrO_2.

i) In cases of N-ZnO or N-SnO_2 materials, substitutional impurities are reported indicating that nitrogen incorporation in these oxides follow a different path with respect to the N-ZT.[23,25,43]

ii) Concerning the parent oxides, more puzzling is the comparison with the ZrO_2. Here in fact, despite several works on nitrogen doped ZrO_2 reported in the literature, no EPR signals have been reported to the best of our knowledge.[17,56-59] This fact again suggests that, also in this case, the nature of the nitrogen impurity is remarkably different respect to the N-$ZrTiO_4$ case.

iii) As far as the second parent oxide (TiO_2) is concerned, both the forms of nitrogen, interstitial and substitutional, have been described even though most of these results derive from X-ray photoelectron spectroscopy, a technique with, in some cases, conflicting conclusions. This is particularly delicate when XPS is used to prove the presence of interstitial N dopants. This is due to the fact that many nitrogen containing species, which can represent by-products of the synthesis, are characterized by a core level binding energy similar to that of interstitial nitrogen.[51,60-62] In spite of this, the paramagnetic nitrogen impurity reported for this oxide is unambiguously assigned due to the interstitial form of nitrogen which strictly resembles the nitrogen impurity in $ZrTiO_4$.[20,63,64] We speculate that such similarity is a direct consequence of the similarity of the structural features of the two oxides. This conclusion is also supported by the fact that in other kinds of nitrogen doped titanates, with structural features different from those of $ZrTiO_4$, XPS data indicate the presence of substitutional nitrogen.[65,66]

It is worth to mention however that in the case of N-SnO_2, even though the material is characterized by the rutile structure, the paramagnetic nitrogen impurity has substitutional character.[25] This indicates therefore that the solely structural affinity does not represent a general rule to predict which form of paramagnetic nitrogen impurity is more stable in an oxide.

4. Conclusions

In the present work it has been shown (optical spectra and DFT) that as far as the electronic structure of N-$ZrTiO_4$ is concerned, the doping procedure does not affect the separation between the valence band and the conduction band being the experimental absorption edge unchanged with respect to the bare oxide (E_g = 3.6 eV). The computed electronic band structure indicates the formation, in N-$ZrTiO_4$, of localized states, which lie above the valence band. The presence of these intra band gap states explains the visible light absorption properties of the material (Scheme 1A-B). The N intra band gap states can be either singly or doubly occupied with the formation, beside the paramagnetic species $N^{\bullet}$, of the corresponding diamagnetic counterpart (N^{-}). The presence of N dopants facilitates the formation of oxygen vacancies, which in turn transfer the excess electrons to the N intra ban gap state, reducing $N^{\bullet}$ to N^{-}. This model for the electronic structure of the doped solid was confirmed by both the EPR measurements performed under irradiation (Scheme 1C) and the behaviour of the material upon annealing under vacuum (Scheme 1D). In the first case the visible light illumination affects the ratio between paramagnetic and diamagnetic population in the solid via preferential electron excitation, into the conduction band, from the more abundant doubly occupied states. In the second case, when excess electrons in the solid are generated via oxygen depletion, they are trapped by the nitrogen states affecting, again, the paramagnetic population in the material.

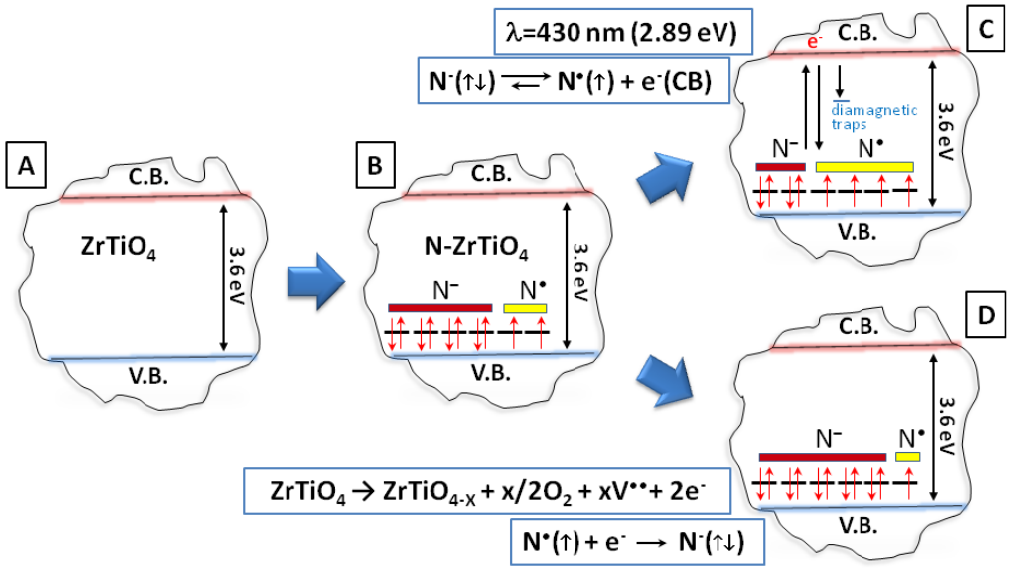

Scheme 1. Proposed model for the description of the electronic and paramagnetic properties of N-doped $ZrTiO_4$ (interstitial N dopant). A) electronic structure of bare $ZrTiO_4$. B) electronic structure of N-$ZrTiO_4$. C) effect of visible light irradiation on the paramagnetic population in the doped solid. D) effect of the thermal annealing in vacuum on the paramagnetic population in the doped solid.

Acknowledgements

Financial support from the Italian MIUR through the PRIN Project 2015K7FZLH, SMARTNESS "Solar driven chemistry: new materials for photo- and electro-catalysis" is gratefully acknowledged. The CINECA-LISA grant n° HPL13PITRY and HPL13PYS1C, 2016-2017, for high-performance computing resources is also acknowledged.

References

1. R. Asahi, T. Morikawa, H. Irie and T. Ohwaki, *Chem. Rev.*, 2014, **114**, 9824-9852.
2. B. Chavillon, L. Cario, A. Renaud, F. Tessier, F. Chevire, M. Boujtita, Y. Pellegrin, E. Blart, A. Smeigh, L. Hammarstrom, F. Odobel and S. Jobic, *J. Am. Chem. Soc.*, 2012, **134**, 464-470.
3. K. Wu, J. Jiang, K. Tang, S. Gu, J. Ye, S. Zhu, K. Lu, M. Zhou, M. Xu, R. Zhang and Y. Zheng, *J. Magn. Magn. Mater.*, 2014, **355**, 51-57.
4. X. Yang, A. Wolcott, G. Wang, A. Sobo, R. C. Fitzmorris, F. Qian, J. Z. Zhang and Y. Li, *Nano Lett.*, 2009, **9**, 2331-2336.
5. S. Livraghi, M. C. Paganini, E. Giamello, A. Selloni, C. Di Valentin and G. Pacchioni, *J. Am. Chem. Soc.*, 2006, **128**, 15666-15671.
6. H. von Wenckstern, H. Schmidt, M. Brandt, A. Lajn, R. Pickenhain, M. Lorenz, M. Grundmann, D. M. Hofmann, A. Polity, B. K. Meyer, H. Saal, M. Binnewies, A. Börger, K. D. Becker, V. A. Tikhomirov and K. Jug, *Prog. Solid State Chem.*, 2009, **37**, 153-172.
7. T. M. Suzuki, S. Saeki, K. Sekizawa, K. Kitazumi, N. Takahashi and T. Morikawa, *Appl. Catal., B*, 2017, **202**, 597-604.
8. D. O. Scanlon and G. W. Watson, *J. Mater. Chem.*, 2012, **22**, 25236-25245.
9. J. L. Lyons, A. Janotti and C. G. Van de Walle, *Appl. Phys. Lett.*, 2009, **95**, 252105.
10. S. Livraghi, N. Barbero, S. Agnoli, C. Barolo, G. Granozzi, F. Sauvage and E. Giamello, *Phys. Chem. Chem. Phys.*, 2016, **18**, 22617-22627.
11. S. B. Ogale, *Adv. Mater.*, 2010, **22**, 3125-3155.
12. I. S. Elfimov, A. Rusydi, S. I. Csiszar, Z. Hu, H. H. Hsieh, H. J. Lin, C. T. Chen, R. Liang and G. A. Sawatzky, *Phys. Rev. Lett.*, 2007, **98**, 137202.
13. L. Shen, R. Q. Wu, H. Pan, G. W. Peng, M. Yang, Z. D. Sha and Y. P. Feng, *Phys. Rev. B*, 2008, **78**, 073306.
14. C. Gómez-Polo, S. Larumbe and M. Monge, *J. Alloys Compd.*, 2014, **612**, 450-455.
15. L. X. Guan, J. G. Tao, C. H. A. Huan, J. L. Kuo and L. Wang, *Appl. Phys. Lett.*, 2009, **95**, 012509.
16. X. Tan, C. Chen, K. Jin and Y. Gao, *Phys. B*, 2013, **412**, 91-93.
17. H. Zhu, J. Li, K. Chen, X. Yi, S. Cheng and F. Gan, *Scientific Reports*, 2015, **5**, 8586.
18. E. Albanese, M. Leccese, C. Di Valentin and G. Pacchioni, *Scientific Reports*, 2016, **6**, 31435.
19. E. Albanese and G. Pacchioni, *Phys. Chem. Chem. Phys.*, 2017, **19**, 3279-3286.
20. C. Di Valentin, E. Finazzi, G. Pacchioni, A. Selloni, S. Livraghi, M. C. Paganini and E. Giamello, *Chem. Phys.*, 2007, **339**, 44-56.
21. A. M. Czoska, S. Livraghi, M. C. Paganini, E. Giamello, C. Di Valentin and G. Pacchioni, *Phys. Chem. Chem. Phys.*, 2011, **13**, 136-143.
22. F. Napoli, M. Chiesa, E. Giamello, M. Fittipaldi, C. Di Valentin, F. Gallino and G. Pacchioni, *J. Phys. Chem. C*, 2010, **114**, 5187-5192.
23. F. Gallino, C. Di Valentin, G. Pacchioni, M. Chiesa and E. Giamello, *J. Mater. Chem.*, 2010, **20**, 689-697.
24. G. Barolo, S. Livraghi, M. Chiesa, M. C. Paganini and E. Giamello, *J. Phys. Chem. C*, 2012, **116**, 20887-20894.
25. E. Albanese, C. Di Valentin, G. Pacchioni, F. Sauvage, S. Livraghi and E. Giamello, *J. Phys. Chem. C*, 2015, **119**, 26895-26903.
26. M. Chiesa, M. C. Paganini, E. Giamello, D. M. Murphy, C. Di Valentin and G. Pacchioni, *Acc. Chem. Res.*, 2006, **39**, 861-867.
27. H. W. Seidel, H.C., *EPR and ANDOR Spectroscopy of Colour centres in Alkali Halide Crystals. In Physics of color Centres*, Beall Fowler, W., Ed, Academic: New York, 1968.

28. S. Pol, V. Pol, A. Gedanken, G. Spijksma, J. Grinblat, R. K. Selvan, V. Kessler, G. Seisenbaeva and S. Gohil, *J. Phys. Chem. C*, 2007, **111**, 2484-2489.
29. D.-S. Kim, D.-H. Park, G.-D. Kim and S.-Y. Choi, *Met. Mater. Int.*, 2004, **10**, 361-365.
30. P. Lessing, Z. Yang, G. Miller and H. Yamada, *J. Electrochem. Soc.*, 1988, **135**, 1049-1057.
31. Y. Park, *Phys. Rev. B*, 2000, **62**, 8794-8801.
32. L. Lutterotti, S. Matthies, H. R. Wenk, A. S. Schultz and J. W. Richardson, *J. Appl. Phys.*, 1997, **81**, 594-600.
33. http://maud.radiographema.com
34. A. Adamski, T. Spałek and Z. Sojka, *Res. Chem. Intermed.*, 2003, **29**, 793-804.
35. A. D. Becke, *J. Chem. Phys.*, 1993, **98**, 5648-5652.
36. C. Lee, W. Yang and R. G. Parr, *Phys. Rev. B*, 1988, **37**, 785-789.
37. R. Dovesi, V. Saunders, C. Roetti, R. Orlando, C. Zicovich-Wilson, F. Pascale, B. Civalleri, K. Doll, N. Harrison and I. Bush, *CRYSTAL14 Users Manual*, University of Torino,Torino, 2014.
38. P. J. Hay and W. R. Wadt, *J. Chem. Phys.*, 1985, **82**, 299-310.
39. R. E. Newnham, *J. Am. Ceram. Soc.*, 1967, **50**, 216-216.
40. V. Polliotto, E. Albanese, S. Livraghi, P. Indyka, Z. Sojka, G. Pacchioni and E. Giamello, *J. Phys. Chem. C*, 2017, **121,** , 5487-5497.
41. J. A. J. Fitzpatrick, F. R. Manby and C. M. Western, *J. Chem. Phys.*, 2005, **122**, 084312–084324.
42. S. Livraghi, M. C. Paganini, M. Chiesa and E. Giamello, *Res. Chem. Intermed.*, 2007, **33**, 739-747.
43. N. Y. Garces, L. J. Wang, N. C. Giles, L. E. Halliburton, G. Cantwell and D. B. Eason, *J. Appl. Phys.*, 2003, **94**, 519-524.
44. C. Di Valentin, G. Pacchioni and A. Selloni, *Phys. Rev. B*, 2004, **70**, 085116.
45. S. Livraghi, A. M. Czoska, M. C. Paganini and E. Giamello, *J. Solid State Chem.*, 2009, **182**, 160-164.
46. M. Takeuchi, Y. Shimizu, H. Yamagawa, T. Nakamuro and M. Anpo, *Appl. Catal., B*, 2011, **110**, 1-5.
47. R. S. Vemuri, M. Noor-A-Alam, S. K. Gullapalli, M. H. Engelhard and C. V. Ramana, *Thin Solid Films*, 2011, **520**, 1446-1450.
48. M. N. Huda, Y. F. Yan, S. H. Wei and M. M. Al-Jassim, *Phys. Rev. B*, 2009, **80**, 115118.
49. X. Sun, R. Long, X. Cheng, X. Zhao, Y. Dai and B. Huang, *J. Phys. Chem. C*, 2008, **112**, 9861-9864.
50. S. S. Pan, G. H. Li, L. B. Wang, Y. D. Shen, Y. Wang, T. Mei and X. Hu, *Appl. Phys. Lett.*, 2009, **95**, 222112
51. S. Livraghi, M. R. Chierotti, E. Giamello, G. Magnacca, M. C. Paganini, G. Cappelletti and C. L. Bianchi, *J. Phys. Chem. C*, 2008, **112**, 17244-17252.
52. S.-K. Joung, T. Amemiya, M. Murabayashi and K. Itoh, *Appl. Catal., A*, 2006, **312**, 20-26.
53. X. Chen and C. Burda, *J. Phys. Chem. B*, 2004, **108**, 15446-15449.
54. O. Diwald, T. L. Thompson, E. G. Goralski, S. D. Walck and J. T. Yates, *J. Phys. Chem. B*, 2004, **108**, 52-57.
55. J. M. Mwabora, T. Lindgren, E. Avendaño, T. F. Jaramillo, J. Lu, S.-E. Lindquist and C.-G. Granqvist, *J. Phys. Chem. B*, 2004, **108**, 20193-20198.
56. X. Wang, J. C. Yu, Y. Chen, L. Wu and X. Fu, *Environ. Sci. Technol.*, 2006, **40**, 2369-2374.
57. X. F. Qiu, Y. X. Zhao and C. Burda, *Adv. Mater.*, 2007, **19**, 3995-3999.
58. Y. Yu, P. Zhang, Y. Kuang, Y. Ding, J. Yao, J. Xu and Y. Cao, *J. Phys. Chem. C*, 2014, **118**, 20982-20988.
59. H. Sudrajat and S. Babel, *Environ. Sci. Pollut. Res.*, 2016, **23**, 10177-10188.
60. S. Yin, Y. Aita, M. Komatsu, J. Wang, Q. Tang and T. Sato, *J. Mater. Chem.*, 2005, **15**, 674-682.
61. R. Bacsa, J. Kiwi, T. Ohno, P. Albers and V. Nadtochenko, *J. Phys. Chem. B*, 2005, **109**, 5994-6003.
62. R. Asahi and T. Morikawa, *Chem. Phys.*, 2007, **339**, 57-63.
63. Y. Yamamoto, S. Moribe, T. Ikoma, K. Akiyama, Q. Zhang, F. Saito and S. Tero-Kubota, *Mol. Phys.*, 2006, **104**, 1733-1737.
64. E. A. Reyes-Garcia, Y. Sun, K. Reyes-Gil and D. Raftery, *J. Phys. Chem. C*, 2007, **111**, 2738-2748.
65. M. Miyauchi, M. Takashio and H. Tobimatsu, *Langmuir*, 2004, **20**, 232-236.
66. G. Liu, L. Wang, C. Sun, X. Yan, X. Wang, Z. Chen, S. C. Smith, H.-M. Cheng and G. Q. Lu, *Chem. Mater.*, 2009, **21**, 1266-1274.

